Proceedings Paper:
Susmel, L. orcid.org/0000-0001-7753-9176 (2024) Theory of critical distances and notched filament-based 3D-printed components: lessons learned from polymers and concrete. In: Berto, F., Iacoviello, F., De Jesus, A., Torgersen, J. and Vantadori, S., (eds.) Procedia Structural Integrity. Third European Conference on the Structural Integrity of Additively Manufactured Materials (ESIAM23), 04-06 Sep 2023, Porto, Portugal. Elsevier BV , pp. 44-51.

https://doi.org/10.1016/j.prostr.2024.01.006

Available online at www.sciencedirect.com

ScienceDirect

Procedia Structural Integrity 53 (2024) 44–51

Structural Integrity Procedia

www.elsevier.com/locate/procedia

Third European Conference on the Structural Integrity of Additively Manufactures Materials (ESIAM23)

Theory of Critical Distances and notched filament-based 3D-printed components: lessons learned from polymers and concrete

Luca Susmel*

Department of Civil and Structural Engineering, The University of Sheffield, Mappin Street, Sheffield, S1 3JD, UK

Abstract

The present paper reviews the work we did in recent years (Ahmed and Susmel, 2018, 2019; Alanzi et al., 2022) – to use the Theory of Critical Distances to model the detrimental effect of manufacturing defects and voids in 3D-printed concrete/polymers subjected to static loading. The validity and robustness of the proposed approach is assessed against a large number of experimental results that were generated by testing 3D-printed specimens of both concrete and polylactide (PLA) containing manufacturing defects/voids. The sound agreement between experiments and predictive model makes it evident that the Theory of Critical Distances (TCD) is not only a reliable design approach, but also a powerful tool suitable for guiding and informing effectively the additive manufacturing process.

Keywords: Type your keywords here, separated by semicolons ;

1. Introduction

The technologies that are most commonly used to additively-manufacture polymers and concrete make use of an extrusion process where the objects are built layer-by-layer by depositing filaments of the parent material. One of the key features of 3D-printing is that this technology allows objects with intricate designs to be manufactured at a relatively low cost, with this being done by reaching a remarkable level of accuracy in terms of both shape and

* Corresponding author.
E-mail address: l.susmel@sheffield.ac.uk

10.1016/j.prostr.2024.01.006

dimensions. However, the specific features and the intrinsic technological limitations of additive manufacturing result not only in particular material mico-/meso-structural features, but also in defects that are introduced during fabrication. Both material morphology and manufacturing flaws do affect the overall mechanical behaviour and strength of additively manufactured objects.

In this setting, this paper summarises and reviews the work we have done over the last 5 years - Ahmed and Susmel (2018, 2019); Alanzi et al. (2022) - to model via the Theory of Critical Distances the detrimental effect of manufacturing flaws and voids on the static strength of filament-based 3D-printed concrete and polymers.

Nomenclature

a	crack length
a_{eq}	equivalent crack length
d_V	size of the manufacturing voids
B, W, S	concrete specimens' dimensions
F	shape factor
K_{Ic}	plane strain fracture toughness
L	critical distance
Oxy	system of coordinates
r, θ	polar coordinates
σ_{eff}	effective stress estimated according to the Theory of Critical Distances
σ_f	nominal gross stress resulting in the static breakage of cracked materials
σ_g	nominal gross stress
σ_x, σ_y	local normal stresses
τ_{xy}	local shear stress
σ_{FS}	flexural strength
σ_{UTS}	ultimate tensile strength

2. The Theory of Critical Distances and the short/long crack problem

As far as brittle materials are concerned, the Theory of Critical Distances (TCD) postulates that failure takes place when a distance-dependent effective stress, denoted as σ_{eff}, exceeds the material's ultimate tensile strength, σ_{UTS} (Taylor, 2007). As a result, the threshold condition for Mode I static loading can be expressed as follows:

$$\sigma_{eff} = \sigma_{UTS} \tag{1}$$

As outlined in Taylor (2007), the effective stress can be computed through various methodologies, which include the Point, Line, Area, and Volume Methods. Notably, it has been observed that these different formalizations of the TCD yield comparable estimations. For brevity, this discussion will focus solely on the Point Method (PM) and the Line Method (LM), where the corresponding effective stresses can be computed as follows (see Fig. 1):

$$\sigma_{eff} = \sigma_{eff}(\theta = 0, r = L/2) \tag{2}$$

$$\sigma_{eff} = \frac{1}{2L}\int_0^{2L} \sigma_y(\theta = 0, r)dr \tag{3}$$

In definitions (2) and (3), critical distance L is a material property that is estimated via the plane strain fracture toughness, K_{Ic}, and the tensile strength, σ_{UTS}, as follows (Whitney, Nuismer, 1974; Taylor, 2007):

$$L = \frac{1}{\pi}\left(\frac{K_{Ic}}{\sigma_{UTS}}\right)^2 \tag{4}$$

To apply the TCD to model the transition from the short- to the long-crack regime, let's examine a scenario involving a uniaxially loaded infinite plate containing a centrally located through-thickness crack with a semi-length equal to a (Fig. 1a). In accordance with the work of Westergaard (1939), the linear-elastic stress distribution along the crack's bisector (where θ=0 in Fig. 1a) can be approximated using the following equation:

$$\sigma_y(\theta = 0, r) = \frac{\sigma_g}{\sqrt{1-\left(\frac{a}{a+r}\right)^2}} \tag{5}$$

If stress σ_y is determined from Eq. (5) at a distance r from the crack tip equal to L/2 and the failure condition is expressed according to Eq. (1), the PM can be used to model the transition from the short- to the long-crack regime as via the following relationship (Taylor, 1999):

$$\sigma_f = \sigma_{UTS}\sqrt{1-\left(\frac{a}{a+\frac{L}{2}}\right)^2} \tag{6}$$

where σ_f is the value of the nominal stress, σ_g, resulting in the static breakage.

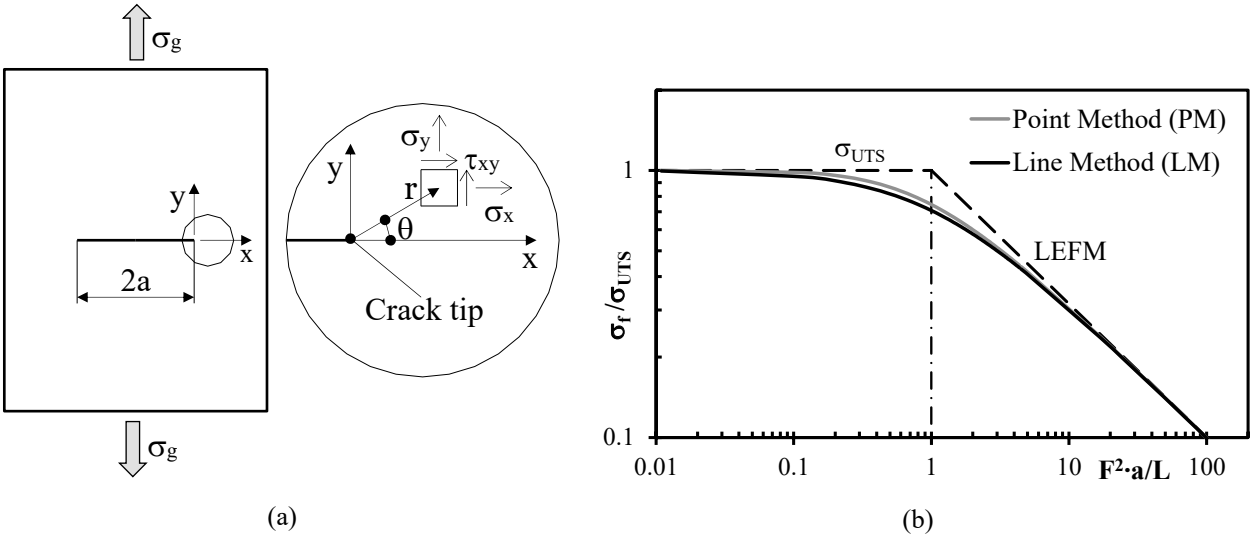

Fig. 1. (a) uniaxially loaded plate containing a central through-thickness crack; (b) normalised Kitagawa-Takahashi diagram and transition from the short- to the long-crack region modelled according to the PM and LM.

Similarly, through the process of averaging σ_y, as determined by Eq. (8), along a linear segment with a length of 2L, the LM effective stress can directly be calculated as:

$$\sigma_{eff} = \frac{1}{2L}\int_0^{2L}\frac{\sigma_g}{\sqrt{1-\left(\frac{a}{a+r}\right)^2}}dr = \sigma_g\sqrt{\frac{a+L}{L}} \tag{7}$$

thus, according to failure condition (1), the transition from the short- to the long-crack regime can directly be modelled as (Taylor, 1999):

$$\sigma_f = \sigma_{UTS}\sqrt{\frac{L}{a+L}} \tag{8}$$

The results calculated from Eq. (6) and Eq. (8) can be displayed together in a normalized Kitagawa-Takashi diagram that plots the σ_f to σ_{UTS} ratio vs. the ratio between equivalent length F^2a and critical distance L. In this setting, F is the shape factor (Anderson, 1995) estimated according to Linear Elastic Fracture Mechanics (LEFM). The normalized Kitagawa-Takashi diagram presented in Fig. 1b shows that both the PM applied according to Eq. (6) and the LM applied according to (8) demonstrate equivalent capabilities in modelling the plain material static strength on the left-hand side and, on the right-hand side, the nominal strength of a cracked plate as estimated through LEFM. To conclude, it is worth pointing out that, in the transition region, the LM is seen to be slightly more conservative than the PM (see Fig. 1b).

3. Theory of Critical Distances and polylactide (PLA) printed with different in-fill levels

Consider the plain strip of additively manufactured (AM) PLA shown in Fig. 2a. This strip is assumed to be fabricated by using a fused deposition modeling 3D printer where the in-fill level is set below 100%. An infill density lower than 100% results in internal manufacturing voids having equivalent size equal to d_V (as defined in Fig. 2a). This plain strip is assumed to be loaded in tension, where the applied fictitious stress is denoted as σ_f (i.e., the material is assumed to be in an incipient failure condition).

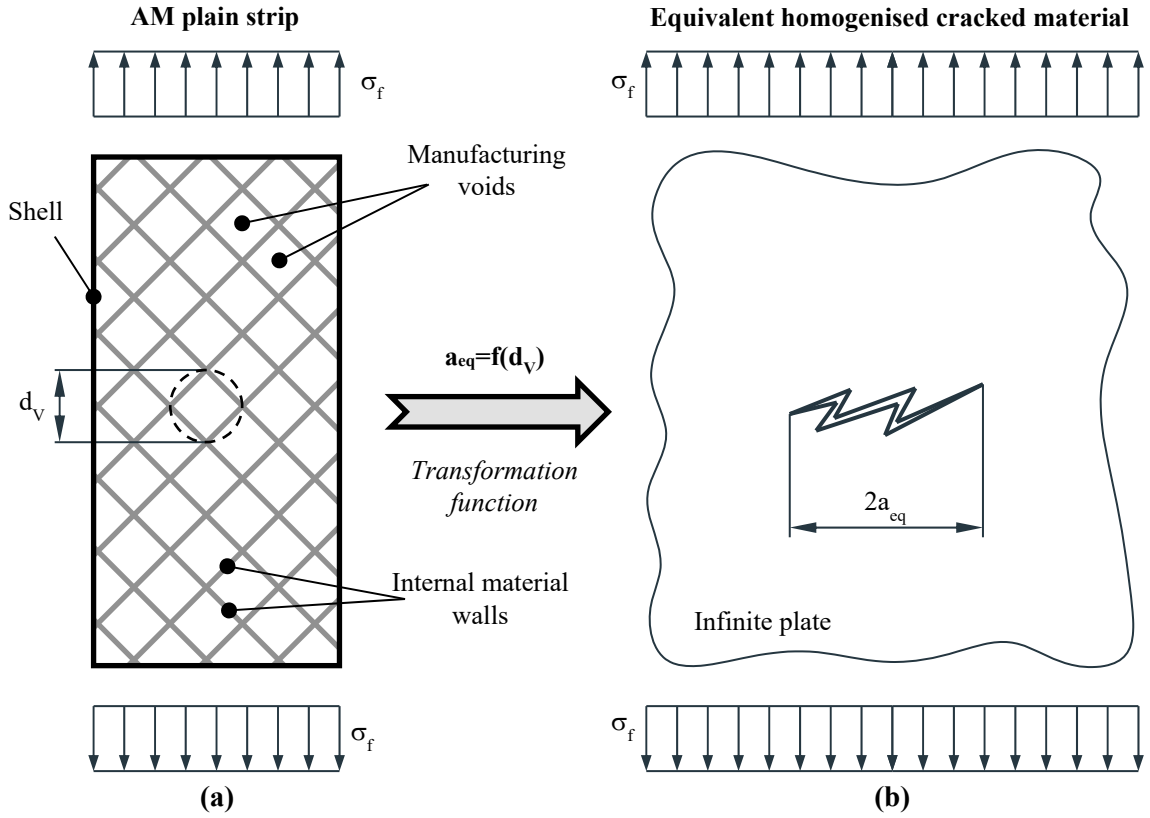

Fig. 2. Object 3D-printed with an in-fill level lower than 100% (a) and equivalent homogenised cracked material (b).

Now, imagine an infinite plate, as depicted in Fig. 2b, made of a continuum, homogeneous, isotropic, linear-elastic material. The ultimate tensile strength, σ_{UTS}, and fracture toughness, K_{Ic}, for this material are hypothesized to be determined experimentally by testing 100% in-fill specimens of the same AM material used to fabricate the strip in Fig. 2a. The infinite plate in Fig. 2b also contains a central through-thickness crack with a semi-length of a_{eq}. The length of this crack is adjusted so that the plate in Fig. 2b fails when the applied nominal remote stress equals the

fictitious failure stress, σ_f, that would lead to the failure of the AM plain strip of Fig. 2a. Consequently, the plate with the central through-thickness crack of Fig. 2b is also considered to be in the incipient failure condition. It is important to note that, since the component seen in Fig. 2b is schematized as an infinite plate containing a central through-thickness crack, the corresponding LEFM shape factor is invariably to unity, regardless of the crack's semi-length, a_{eq}.

Based on the hypotheses formed above, LEFM postulates that the cracked plate seen in Fig. 2b fails when the associated stress intensity factor equals the material's fracture toughness. As a result, the failure condition for the homogenized equivalent cracked material can be expressed as follows:

$$K_{Ic} = \sigma_f \sqrt{\pi a_{eq}} \tag{9}$$

Assume now that there is a univocal link between semi-length a_{eq} (Fig. 2b) and the size, d_V, of the manufacturing voids (Fig. 7a), i.e. (Ahmed, Susmel, 2019):

$$a_{eq} = f(d_V) \tag{10}$$

where $f(d_V)$ is a transformation function able to turning the 3D-printed plain strip depicted in Fig. 2a into the equivalent cracked material as sketched in Fig. 2b.

Consider now the PM and the LM formalised to assess the case of a through-thickness crack in an infinite plate loaded in tension – see Eq. (6) and Eq. (8). If the generic semi-crack length is replaced with the equivalent semi-crack length, it is straightforward to obtain (Ahmed, Susmel, 2019):

$$\sigma_f = \sigma_{UTS} \sqrt{1 - \left(\frac{a_{eq}}{a_{eq} + \frac{L}{2}} \right)^2} = \sigma_{UTS} \sqrt{1 - \left[\frac{f(d_V)}{f(d_V) + \frac{L}{2}} \right]^2} \tag{11}$$

$$\sigma_f = \sigma_{UTS} \sqrt{\frac{L}{a_{eq} + L}} = \sigma_{UTS} \sqrt{\frac{L}{f(d_V) + L}} \tag{12}$$

In the above relationships σ_{UTS} is to be determined by testing specimens manufactured by setting the in-fill level equal to 100%. In a similar way, L in Eq. (11) and (12) is calculated via definition (4) where the used values for σ_{UTS} and K_{Ic} are those associated with an in-fill level of 100%.

To formalise transformation function (10), the hypothesis can be formed that the link between a_{eq} and d_V can be described successfully by using a simple linear relationship so that (Ahmed, Susmel, 2019):

$$a_{eq} = f(d_V) = k_t \cdot d_V \tag{13}$$

In relationship (13), k_t is a dimensionless transformation constant that can be determined experimentally from the strength of specimens manufactured with an in-fill level lower than 100%.

In order to check the accuracy of Eqs (11) and (12), a large number of dog-bone specimens were tested under quasi-static tensile loading. The specimens used in this study were fabricated, through an Ultimaker 2 Extended+ 3D printer, by employing a 2.85mm diameter white filaments of New Verbatim PLA. The manufacturing parameters adhered to the following specifications: a nozzle size of 0.4 mm, nozzle temperature set to 240°C, build-plate temperature maintained at 60°C, a printing speed of 30 mm/s, a layer height of 0.1 mm, and a shell thickness of 0.4 mm. The specimens were all manufactured flat on the build-plate by setting the angle, θ_p, between printing direction and samples' longitudinal axis equal to 0°, 30°, and 45°. In-fill levels between 10%-100% were used to investigate the detrimental effect of the internal manufacturing voids. The thickness of both the shell and the internal walls in the specimens containing internal manufacturing voids was set equal to 0.4 mm. The material ultimate tensile strength and fracture toughness for an in-fill level equal to 100% were determined to be equal to 42.9 MPa and to 3.7 MPa $m^{1/2}$, respectively, resulting in a critical distance value, L, equal to 2.4 mm. For a detailed description of these experimental results, the reader is referred to the papers by Ahmed and Susmel (2018, 2019).

In order to apply Eqs (11) and (12), the results from the specimens additively manufactured with an in-fill level equal to 80% were used to estimate k_t in Eq. (13). This calibration process resulted in a k_t value equal to 35.5 for the PM and to 33.1 for the LM.

The Kitagawa–Takahashi diagrams of Fig. 3 summarise the overall accuracy that was obtained by using the PM and the LM in the form of Eqs (11) and (12) to estimate the static strength of the plain specimens of AM PLA having in-fill level lower than 100%. These charts suggest that the use of the proposed approach yields a remarkable level of accuracy down to an in-fill density of 30%. However, when the fill density decreases to 20% and 10%, the resulting estimates noticeably deviate from the anticipated trend. This observation aligns with expectations, as 3D-printed objects tend to exhibit lattice-like characteristics when the mesh of their internal walls becomes coarse. Consequently, using the concept of an equivalent homogenized material to simulate the mechanical behaviour and strength of 3D-printed objects with very low fill densities is no longer justifiable. This effectively establishes the lower limit for the applicability of the proposed methodology in practical scenarios.

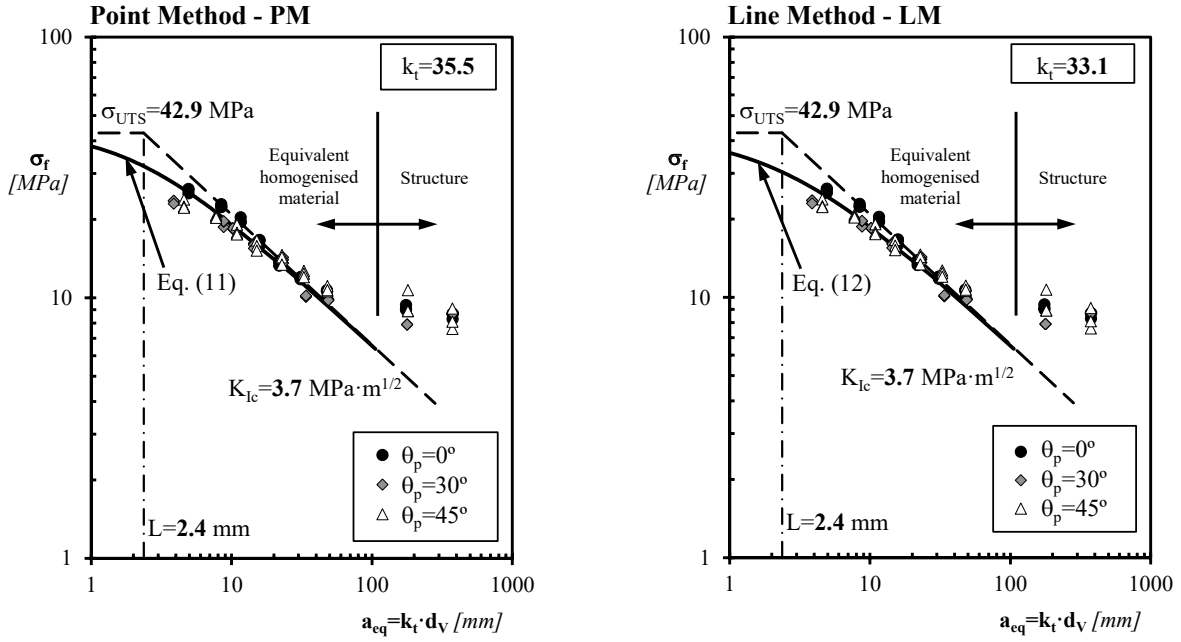

Fig. 3. Accuracy of the PM and LM in estimating the static strength of PLA 3D-printed with different in-fill levels (Ahmed, Susmel, 2019).

4. Theory of Critical Distances and and 3D-printed concrete containing defect

The concrete mix used to manufacture the specimens included 52.5N CEM I Portland Cement, fly ash, silica fume, sand, water, a superplasticizer based on polycarboxylate ester, and a retarder based on amino tris (methylene phosphonic acid). The specimens being tested were 3D-printed using an ABB IRR 6640 6-axis robot, with concrete extrusion occurring at rates of 200, 225, and 250 mm/s through a 10 mm diameter nozzle. The manufacturing process was optimised to achieve a layer height of 6 mm with a pump flow rate of 0.72 L/min.

Following 3D printing, the slabs were covered for 24 hours and subsequently cured for 28 days. The higher print speeds of 225 and 250 mm/s were intentionally used to introduce manufacturing defects due to volume mismatch. After post-manufacturing curing, the concrete slabs were saw-cut to create rectangular beams with varying width, W, within the range of 44-53 mm and thickness, B, within the range of 34-56 mm (see Fig. 4). The beams were cut in a way that their printing direction was either parallel (θ_p=0°) or perpendicular (θ_p=90°) to the longitudinal axis of the specimen.

The specimens were tested using a three-point bending setup (Fig. 4) under a displacement rate set at 33.3 N/sec. The span, S, between the lower rollers was adjusted to either 60 mm, 80 mm, or 100 mm.

In addition to un-notched samples (Fig. 4a), three other configurations were considered as follows.

1. Specimens with crack-like notches varying in depth, a, from 2 to 27 mm, which were created using a circular tip blade with a thickness of 2.6 mm (Fig. 4b).

2. Specimens to investigate the impact of the surface roughness resulting from the filament deposition process, where the valleys of the surface texture were treated as cracks. The depth, a, of these equivalent cracks ranged from 1.2 mm to 3.5 mm, depending on the maximum valley depth below the filament peaks in the vicinity of the failure location (Fig. 4c).

3. A final set of specimens was manufactured to introduce 3D printing-induced flaws primarily on the side undergoing tensile stress during testing (Fig. 4d). These defects were considered interconnected, resulting in an equivalent crack with a length, a, defined as shown in Fig. 4d.

For a comprehensive description of the experimental results obtained following the outlined experimental procedure, readers are directed to a recent publication by Alanazi et al. (2022).

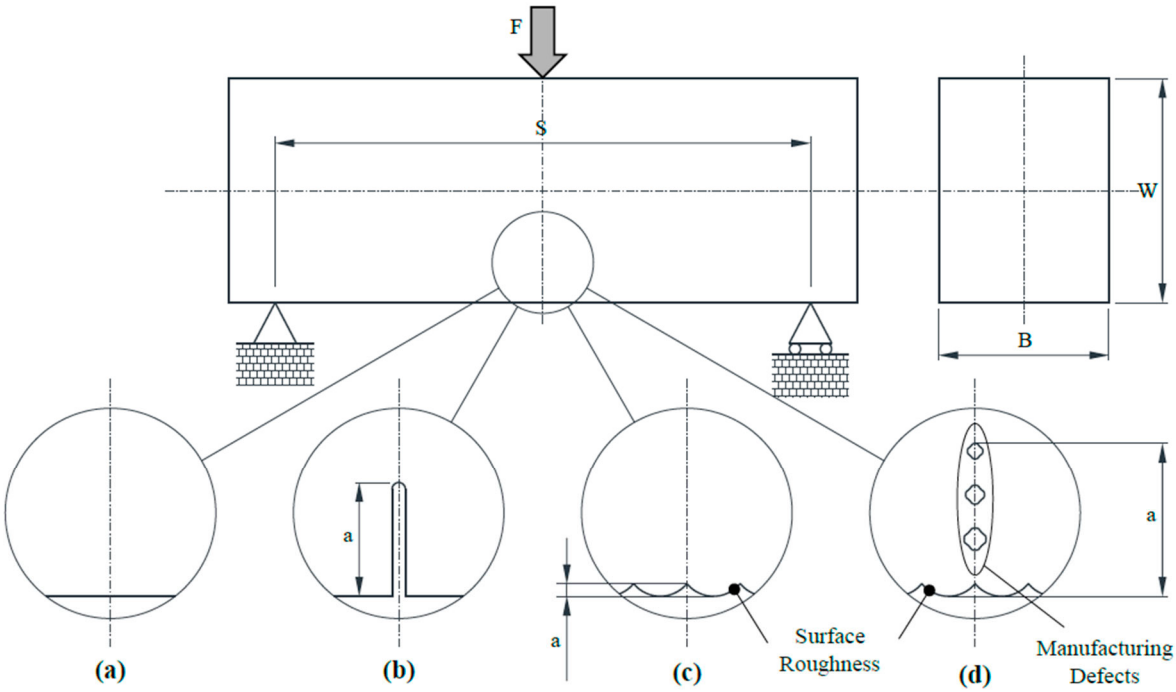

Fig. 4. 3D-printed specimens tested under three-point bending: plain specimen (a); specimen containing a saw-cut crack-like sharp notch (b); specimen weakened by surface roughness (c); specimen weakened by manufacturing defects (d) – (Alanazi et al., 2022).

All tested specimens were modelled numerically using Finite Element (FE) code ANSYS® to determine the corresponding linear-elastic stress distributions. The samples were modelled as single edge notched bend beams with notch tip radius equal to zero. Any specimen was modelled by using the actual geometrical dimensions, with the crack length, a, for the various cases being defined as summarised in Fig. 4. The stress analysis was conducted using two-dimensional elements with thickness (i.e., PLANE183). The mesh density in the zero-radius notch tip region was progressively increased to ensure convergence in calculating the stress intensity factor. The linear-elastic stress fields derived from these FE models were used not only to calculate the stress intensity factors but also to determine the shape factors following the standard procedure recommended by Anderson (1995).

Based on the experimental results obtained, the plain material's flexural strength, σ_{FS}, and plane strain fracture toughness, K_{Ic}, were estimated to be 13.7 MPa and 1.2 MPa·m$^{1/2}$, respectively. With σ_{FS} and K_{Ic} determined for the investigated 3D-printed concrete, Eq. (4) was employed to compute the critical distance value (where σ_{UTS} was directly replaced with σ_{FS}). This straightforward calculation yielded a critical distance, L, of 2.4 mm.

These material constants, in combination with the experimental results, were then utilized to construct the Kitagawa–Takahashi diagram depicted in Fig. 5. This diagram provides a concise representation of the overall accuracy of the TCD used in the form of both the PM, Eq. (6), and the LM, Eq. (5). The diagram of Fig. 5 demonstrates that, in the presence of 3D-printed concrete as well, the application of the TCD resulted in a remarkable level of accuracy, which remained consistent regardless of the specific type of local stress raiser being considered.

5. Conclusions

The TCD is seen to be successful in modelling the detrimental effect of manufacturing defects and voids in filament-based 3D-printed concrete/polymers subjected to static loading. This result is certainly remarkable since it demonstrates that the same theoretical formulation can directly be used to assess effectively the detrimental effect of local stress concentrators in two additively manufactured materials that are different in terms of constitutive components, microstructural features, and mechanical behaviour.

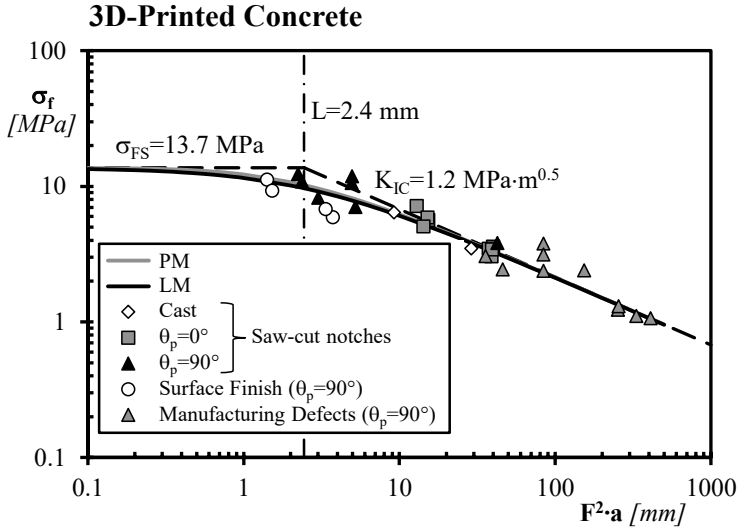

Fig. 5. Accuracy of the PM and LM in estimating the static strength of 3D-printed concrete (Alanazi et al., 2022).

References

Ahmed, A. A., Susmel, L., 2018. A material length scale based methodology to assess static strength of notched additively manufactured polylactide (PLA). Fatigue and Fracture of Engineering Materials and Structures 41(10), 2071-2098.

Ahmed, A. A., Susmel, L., 2019. Static assessment of plain/notched polylactide (PLA) 3D-printed with different in-fill levels: equivalent homogenised material concept and Theory of Critical Distances. Fatigue and Fracture of Engineering Materials and Structures 42, 883–904.

Alanazi, N., Kolawole, J.T., Buswell, R., Susmel, L., 2022. The Theory of Critical Distances to assess the effect of cracks/manufacturing defects on the static strength of 3D-printed concrete. Engineering Fracture Mechanics 269, 108563.

Anderson, T. L., 1995. *Fracture mechanics: Fundamentals and applications*. Boca Raton, CRC Press.

Taylor, D., 1999. Geometrical effects in fatigue: a unifying theoretical model. International Journal of Fatigue 21, 413-420.

Taylor, D., 2007. *The Theory of Critical Distances: A New Perspective in Fracture Mechanics*. Elsevier Science, Oxford, UK.

Westergaard, H. M., 1939. Bearing pressures and cracks. Journal of Applied Mechanics A 61, 49-53.

Whitney, J.M., Nuismer, R.J., 1974. Stress fracture criteria for laminated composites containing stress concentrations. Journal of Composite Materials 8, 253-265.